

Many-body theory of the nuclear quadrupole coupling in the boron atom

James E. Rodgers and T. P. Das

Department of Physics, State University of New York, Albany, New York 12222

(Received 10 October 1974)

The linked-cluster many-body perturbation theory is utilized to obtain an accurate value of the electric field gradient for the lowest ${}^2P_{3/2}$ state of atomic boron. This diagrammatic method permits us to examine the relative importance of angular-polarization and dynamic correlation effects on the electric field gradient. Also, a detailed comparison with another many-body theory of contributions classified by Hartree-Fock labels is made. The resulting quadrupole shielding factor $R = 0.0989 \pm 0.0099$ yields a field gradient $q = 0.27957 \pm 0.00276$ a.u. Finally, we obtain from the quadrupole coupling constants the nuclear quadrupole moments of ${}^{10}\text{B}$ and ${}^{11}\text{B}$ as $(8.543 \pm 0.104) \times 10^{-2}$ and $(4.099 \pm 0.047) \times 10^{-2}$ b, respectively.

I. INTRODUCTION

A knowledge of the quadrupole moments of nuclei is useful for several reasons. Prominent among these is that one can utilize the nuclear quadrupole moment Q to extract from the quadrupole coupling constants in molecular and solid-state systems, electric field gradients at the nuclear sites. The field gradients themselves are useful parameters to test our knowledge of the electronic structures of these systems. Quite often the field gradient exhibits sensitivity to the fine details of the electronic wave function. Additionally the nuclear quadrupole moments are also important parameters from the point of view of theories of nuclear structure and of course NMR spectroscopy. At the present time, the most convenient and widely employed procedure to obtain nuclear quadrupole moments is to extract them from measured quadrupole coupling constants in isolated atoms using calculated field gradients.

The evaluation of the field gradient for an atomic state leads us to the phenomenon of shielding¹ of the outer-electron field gradient by the inner cores, an effect that has been widely studied in the framework of one-electron theory. In the present investigation, we study the field gradient and consequently the shielding by the linked-cluster many-body perturbation theory (LCMBPT). By this investigation, not only do we want to derive an accurate value of the electric field gradient and hence the nuclear quadrupole moment, but also obtain an understanding of the convergence of the perturbation approach and the role of correlation effects on the shielding. Such effects are of great importance in boron due to the strong correlation between $2p$ and $2s$ electrons. Several investigations of the single particle and correlation contributions have been reported,^{9,12,16-22} in the litera-

ture by various one-electron and configuration-interaction procedures, including the role of three-electron correlations.¹² The relationship between our LCMBPT results and these earlier results will be discussed in detail in Sec. III. In the case of magnetic hyperfine interactions, particularly of the contact type, the relative importance of correlation effects is accentuated by the cancellation between different core contributions.²⁻⁴

In Sec. II we shall describe the basis set for the LCMBPT calculation and present the most significant diagrammatic contributions to the quadrupole shielding constant R . Section III will involve a discussion of these results and detailed comparisons with previous calculations by other procedures.

II. DIAGRAMS AND RESULTS

Since the LCMBPT method has been thoroughly discussed in the literature,⁵⁻⁷ we will only describe those points that are of special relevance to the present calculation and to the boron atom. First, the single-particle basis sets were generated⁴ by a numerical integration of the following radial differential equation appropriate for the $1s^2 2s^2 2p_1^+$, ${}^2P_{3/2}$ configuration:

$$\left(-\frac{1}{2} \frac{d^2}{dr^2} + \frac{l(l+1)}{2r^2} - \frac{5}{r} - \epsilon_{nl} + V_l^{N-1}\right) P_{nl}(r) = 0. \quad (1)$$

The nonlocal V_l^{N-1} potential is represented diagrammatically in Fig. 1 in terms of its matrix elements between arbitrary single-particle states k_l . It is to be noted that the V_l^{N-1} potential for s orbitals is that arising from the above configuration with the omission of the Coulomb and exchange contributions due to one of the $2s$ orbitals. With

$$\begin{aligned}
 \left| \begin{array}{c} k'_s \\ \vdots \\ k_s \end{array} \right| V_i^{N-1} = 2 \left| \begin{array}{c} k'_s \\ \vdots \\ k_s \end{array} \right| \begin{array}{c} 1s^\circ \\ \circ \\ \vdots \\ \circ \end{array} + \left| \begin{array}{c} k'_s \\ \vdots \\ k_s \end{array} \right| \begin{array}{c} 2s^\circ \\ \circ \\ \vdots \\ \circ \end{array} + \left| \begin{array}{c} k'_s \\ \vdots \\ k_s \end{array} \right| \begin{array}{c} 2p^\circ \\ \circ \\ \vdots \\ \circ \end{array} \\
 + \frac{1}{2} \left| \begin{array}{c} k'_s \\ \vdots \\ k_s \end{array} \right| \begin{array}{c} 1s^\circ \\ \circ \\ \vdots \\ \circ \end{array} + \frac{1}{2} \left| \begin{array}{c} k'_s \\ \vdots \\ k_s \end{array} \right| \begin{array}{c} 2p^\circ \\ \circ \\ \vdots \\ \circ \end{array}
 \end{aligned}$$

$$\begin{aligned}
 \left| \begin{array}{c} k'_l \\ \vdots \\ k_l \end{array} \right| V_i^{N-1} = 2 \left| \begin{array}{c} k'_l \\ \vdots \\ k_l \end{array} \right| \begin{array}{c} 1s^\circ \\ \circ \\ \vdots \\ \circ \end{array} + 2 \left| \begin{array}{c} k'_l \\ \vdots \\ k_l \end{array} \right| \begin{array}{c} 2s^\circ \\ \circ \\ \vdots \\ \circ \end{array} \\
 + \left| \begin{array}{c} k'_l \\ \vdots \\ k_l \end{array} \right| \begin{array}{c} 1s^\circ \\ \circ \\ \vdots \\ \circ \end{array} + \left| \begin{array}{c} k'_l \\ \vdots \\ k_l \end{array} \right| \begin{array}{c} 2s^\circ \\ \circ \\ \vdots \\ \circ \end{array}
 \end{aligned}$$

FIG. 1. Matrix elements, $\langle k'_l | V_i^{N-1} | k_l \rangle$, of the V_i^{N-1} potentials for the $1s^2 2s^2 2p_1^+ 2p_{3/2}$ configuration of boron.

this choice, the $1s$ orbitals will not see the proper Hartree-Fock potential and require certain corrections discussed below. In addition, we have used a spin-restricted potential as indicated by the factors $\frac{1}{2}$ in front of the exchange contribution with the $2p$ orbital.

The V_i^{N-1} potential used for the $l=1, 2, 3$ orbitals does not suffer from either of the above constraints, being the appropriate potential for the $2p$ orbital or any virtual orbital obtained by removing the $2p$. However, when a $2s$ electron is excited to any $l=1, 2, 3$ state, in particular to k_d which is of special importance for the shielding problem, we shall anticipate that certain potential laddering corrections will be needed. Such correction to diagrams exhibiting a $2s$ to k_d excitation reflect the fact that the s and d potentials correspond to the respective configurations $1s^2 2s^2 2p k s$ and $1s^2 2s^2 k d$, whereas the virtual configuration in the diagram is $1s^2 2s^2 2p k d$. By using a V_i^{N-1} potential one can, of course, obtain a basis for each l consisting of an infinite number of bound states as well as the continuum states. One advantage of this V_i^{N-1} potential over say, the Hartree-Fock choice, is that the former is physically more meaningful for the excited states. Thus, the excited states at large distances from the nucleus see an effective positive charge instead of a charge that one would get with the V^N Hartree-Fock potential. One thus expects better convergence in the perturbation calculation with the V_i^{N-1} basis set.

In the diagrams which will be presented there are two other operators besides V_i^{N-1} which appear as vertices. The multipolar components of $1/r_{12}$

will appear as the usual dashed line. For the electric field gradient an additional vertex notation is needed. The electric-field-gradient operator is

$$\hat{q} = -2e \sum_{i=1}^N C_0^{(2)}(\theta_i, \phi_i)/r_i^3 \quad (2)$$

with expectation value

$$q_J = \langle J, M_J = J | \hat{q} | J, M_J = J \rangle \quad (3)$$

$$= q_0(1 - R_J), \quad (4)$$

where

$$q_0 = \langle 2p_1 | \hat{q} | 2p_1 \rangle. \quad (5)$$

In Eq. (3), $|J, M_J = J\rangle$ represents the exact many-electron wave function. We have preferred to express all contributions in terms of the quadrupole shielding factor R defined by Eq. (4). Thus, in our diagrams, a wiggly-line vertex with a q is given as a R contribution in percentage. Note that the zero-order (Hartree-Fock) value in electrostatic units in $q_0 = 0.31025$ a.u. or equivalently⁸ 1.00565×10^5 esu/cm³. Our calculations are done for the $J = \frac{3}{2}$ multiplet since the field gradient vanishes in the $J = \frac{1}{2}$ state.

The first-order contributions to R arise from an admixture of d -orbital symmetry to the $1s$ and $2s$ states. This d admixture, as shown in Fig. 2, comes from the direct Coulomb and exchange interactions with the $2p_1$ occupied state where the M_s ($1s$ or $2s$) orbital is promoted to a virtual d_0 orbital. This process is often referred to as angular polarization and results in a net contribution to the field gradient by the polarized s -core orbitals. The R contribution labeled "bare" in Fig. 2 corresponds to the diagram as shown except that the energy of the $1s$ state has been shifted to correct for the use of the V_i^{N-1} potential as mentioned previously. We note that the $1s$ direct contribution is more than twice as large as for $2s$, whereas the exchange contributions are both com-

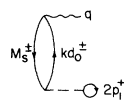
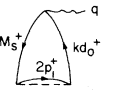
	M_s	Bare (unmodified)	With Ladder corrections	Sternheimer (Ref. 9)	Fully Modified
	1s	8.79	9.391	9.366	9.328
	2s	3.97	3.975	3.847	3.368
	1s	-4.31	-4.653	-4.666	-4.635
	2s	-3.92	-3.806	-3.766	-3.412
NET (DIRECT+EXCHANGE)(%)		4.52	4.907	4.781	4.650

FIG. 2. First-order (0,1) diagrams and their contributions to R (in %) classified by the one-electron state and method of calculation.

parable and of opposite sign to the direct. Also there is near complete cancellation in first order of the $2s$ direct and exchange contributions.

There are a number of ladder-type corrections to these bare diagrams. Most of these arise from the potential as mentioned above. One order of each such ladder correction for the $1s$ direct bare diagram is indicated by the first seven diagrams in Fig. 3. There are corresponding ladder diagrams for $1s$ exchange and the $2s$ cases. The influence of these ladder corrections to all orders is included approximately by applying a geometric-series summation using the ratio γ of the sum of all the first-order corrected diagrams, as in Fig. 3, to the value of the corresponding bare direct diagram in Fig. 2. This means that all possible higher-order mixture corrections, like those indicated by the remaining diagrams in Fig. 3, are taken simultaneously. The contributions of the resulting diagrams with these ladder corrections are shown in the third column of Fig. 2. These effects are more pronounced for the $1s$ state than the $2s$ since in the $2s$ case there is considerable cancellation among ladder effects. We shall continue to refer these ladderized diagrams as first-order effects since they are primarily effects due to the first-order (single-particle) change in the wave functions plus corrections to the single-particle basis states.

These first-order ladderized diagram contributions to R can be compared with the corresponding quantities calculated by the method of Sternheimer.⁹ This method treats the quadrupole interaction as a perturbation to the one-electron states and solves the resulting coupled differential equations numerically. Contributions for boron obtained by this method are given in column four of Fig. 2 and are in excellent agreement with our

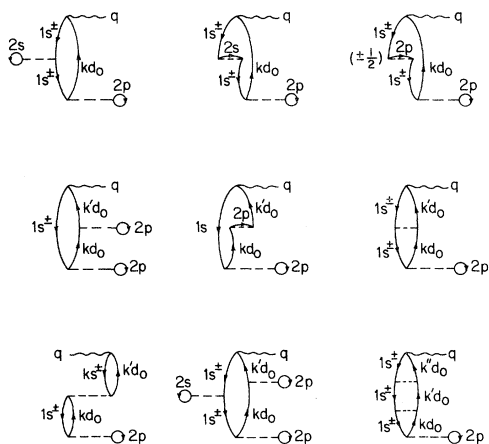


FIG. 3. Examples of ladder corrections to the $1s$ direct diagram of Fig. 2.

results from perturbation theory. We note that the sum of our $1s$ direct and exchange diagrams, here, is 4.740%, whereas the differential equation method gives 4.700%. For $2s$ the corresponding sums are 0.169% and 0.081%, where the difference, in part, reflects the importance of cancellations between the direct and exchange effects on the $2s$ orbital. It should be pointed out that similar agreement between LCMBPT and the Sternheimer method at this level of perturbation was found in the excited 3P state of Be by Ray *et al.*¹⁰

In addition to the potential ladders to the first-order diagrams of Fig. 2 there are higher-order (rearrangement)¹¹ diagrams which are of a different nature. These effects, as indicated in Fig. 4(a)–4(d), arise primarily from double excitations (that is, correlation) between the hole state and other occupied unexcited states. The two time orderings of the vertices in Fig. 4(a) and (b) allow a separation of the two parts, as discussed elsewhere,¹¹ and thus can be summed to all order as a correlation energy correction to the energy denominator, as shown below. Diagrams 4(c) and (d), on the other hand, do not factorize in a similar manner. However, we can approximately treat these as corrections to the denominator of the ladderized first-order diagrams as follows.

The effect of the ladder corrections already discussed (Fig. 3) and the rearrangement diagrams in Figs. 4(a) through 4(d) are given by the modified energy denominator D_2 , namely,

$$D_2 = D_1 + E_c(M_s) + D_1 Q(M_s). \quad (6)$$

In Eq. (6), D_1 is an energy denominator which includes the influence of ladder corrections and is given by

$$D_1 = D_0(1 - \gamma), \quad (7)$$

where D_0 is the denominator in one of the bare diagrams in Fig. 2 and γ is the corresponding

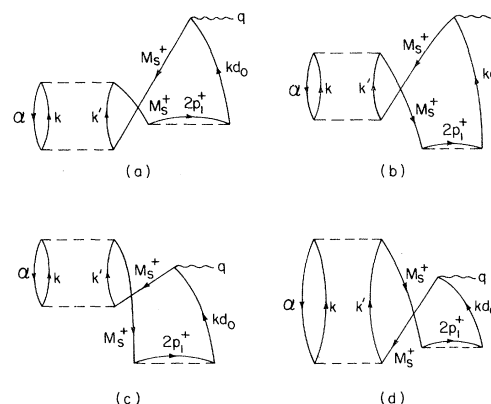


FIG. 4. Form of renormalization-type corrections associated with the (0, 1) diagrams of Fig. 2.

ladderization ratio already discussed. The quantity $E_c(M_s)$ is the sum of all correlation energy diagrams in which hole state M_s can interact. The quantity $Q(M_s)$ is an analogous quantity except that everywhere an energy denominator occurs in the corresponding energy diagram, it is squared in the $Q(M_s)$ case. Thus both contributions, E_c and $D_1 Q$, to D_2 tend to have the same sign and it is found for boron that these are often of comparable significance. We refer to ladderized first-order diagrams having these denominator modifications specified in Eq. (6) as being fully modified.

These fully modified first-order diagrams are given in the last column of Fig. 2. Such correlation-type modification does not change the 1s diagrams significantly but, as expected, do reduce the size of the corresponding 2s contributions by about (10–15)%. It is interesting that such correlation effects change the net 2s contribution from 0.169% for the ladderized diagrams to -0.044% for fully modified. The total first-order (fully modified) contribution to the shielding factor is 4.650%.

In second order there is a large number of diagram contributions to the field gradient. All second-order diagrams have been computed, but we shall restrict our attention to the leading 25 which have bare contributions to R larger than 0.4%.

The leading and possibly most interesting second-order diagram is shown in Fig. 5. This contribution to the shielding factor arises from the correlation between the 2s electrons in which both are promoted to the unoccupied 2p states. Due to the strong correlation among the 2s pair and their large overlap with and similar radial structure to

the 2p orbitals, this contribution is 12.147% when completely unmodified. This is larger than any of the first-order diagrams. However a number of important ladder- and rearrangement-type corrections exist for this case. The hole-hole, hole-particle, and particle-particle ladders, some of which are indicated in Fig. 5, can all be done to all orders exactly. The ladderized value of this diagram is 5.887%, which is almost half of the bare value. This reflects the importance of higher-order interactions among the hole and 2p particle states in this nonspherical open-shell system in which unoccupied near-degenerate (with 2s) orbitals are available for excitation. The virtual excited configuration which is participating here is $1s^2 2p^3$ which is known to have a very significant contribution to other properties of the ground state of boron. In this connection we thought it would be of interest to compute the corresponding field-gradient contribution using a variational configuration-interaction function of the form:

$$\chi(^2R_{3/2}) = C_1 \Phi(1s^2 2s^2 2p_1^+) + C_2 \Phi(1s^2 2p^3). \quad (8)$$

This calculation produced a contribution to R of 5.93% which agrees very well with our ladderized value from perturbation theory, 5.89%.

In addition to ladders we also must consider the rearrangement-type corrections analogous to those computed for the first-order ladderized diagrams. Here we compute the correlation energy correction for a 2s hole with all other occupied states including the other 2s. For each correlation energy term in the modified denominator of the ladderized diagram a ratio like Q in Eq. (6) is also computed. The fully modified diagram in Fig. 5 gives an R contribution of 3.872%. This reduction shows that for correlation sensitive pairs, such as 2s, the rearrangement-like corrections, as computed here, can be quite significant and should not be neglected.

Finally, then, the principal contribution from the 2s pair to the quadrupole shielding factor is 3.872%. This reflects a substantial influence of ladders and correlation effects in higher order.

The remaining 24 leading second-order diagrams are summarized in Fig. 6 and Table I. These diagrams all involve some degree of electronic correlation. The (0, 2) diagrams [Fig. 6(a)–6(f)] have correlation usually between the 2s-2p pair which is combined with either a 2p radial excitation or a 2s angular [Fig. 6(c)] excitation contribution to the field gradient. On the other hand, the (1, 1) diagrams, Fig. 6(g)–6(k), are comprised of two orders of 2s-2s or 2s-2p correlation corrections to the wave function with a contribution to the field gradient occurring in the correlated intermediate state. In the first

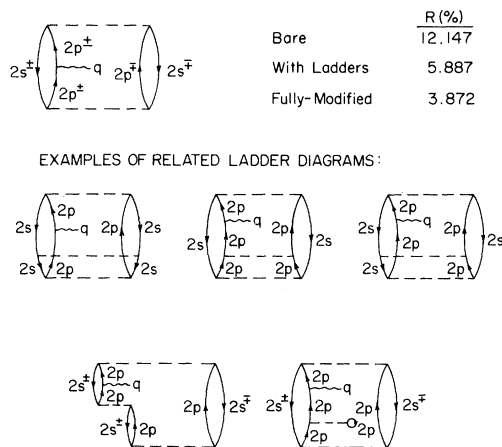


FIG. 5. The principal second-order (1, 1) diagram contributing to R . Results are given for different levels of approximation. Also shown are examples of higher-order ladder diagrams belonging to this (1, 1) case.

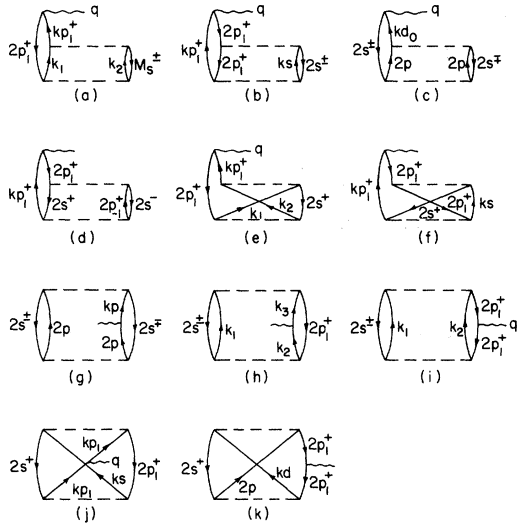


FIG. 6. The leading 24 second-order diagrams. For shielding-constant contributions see Table I.

column of Table I we list the diagrammatic contributions in the completely unmodified form except for two cases. These two cases, Fig. 6(c) and 6(g), are seen to have a part of the diagram which is exactly of the same type as the $2s$ - $2s$ correlation diagram of Fig. 5 and should have the same type of denominator correction as computed there. The correspondingly corrected values of

these two diagrams are given in parentheses in the next to the last column of Table I.

In the last column of Table I we give the contribution after the diagram has been fully ladderized and corrected for rearrangement-type corrections to the hole lines. The ladderization includes, in approximate ways, particle-particle ladders which may involve, in principle, a five-fold integration over the continuum. Such integrations have been done approximately in a way determined by the particular diagram. The technique suggested by Kelly¹¹ was not always found to give meaningful results here and appropriate changes have been introduced. Each diagram is treated separately in detail for higher-order corrections.

From a comparison of contributions in Table I with and without modifications it is seen that the bare diagrams have about equal likelihood of being increased or decreased in magnitude by higher-order modifications. Nevertheless the R contributions of these 24 diagrams is 1.879% in the unmodified form and 0.471% after modification. This reflects a reduction by 1.408% owing to higher-order modifications.

The largest diagrams in Fig. 6 are (6a) with $M_s = 2s^\pm$ and $k_1 = kp$, $k_2 = ks$ and diagram (6b). These diagrams represent similar effects and are seen to be nearly canceling, especially after modifica-

TABLE I. Second-order contributions to R (in percent) corresponding with Fig. 6(a)-6(k).

Part of figure 6	Hole state		Particle states			Bare	Fully modified
	M_s	k_1	k_2	k_3			
(a)	$1s^\pm$	kp	ks			-0.418	-0.468
	$2s^\pm$	kp	ks			-6.211	-7.524
	$1s^\pm$	kd	kp			-1.505	-1.840
	$2s^\pm$	kd	kp			-1.395	-1.326
	$2s^\pm$	ks	kp			-0.522	-0.638
	$2s^\pm$	kf	kd			-0.517	-0.630
	$2s^-$	ks	$2p_1^-$			-0.789	-0.556
	$2s^\pm$	$2p$	kd			-0.426	-0.238
	$2s^\pm$	kd	$2p$			0.944	0.546
(b)					5.646	7.516	
(c)					1.936(1.093)	1.063	
(d)					1.713	1.244	
(e)		kp	ks			0.647	0.696
		ks	kp			1.016	1.099
		kd	$2p$			0.434	0.405
(f)					-0.944	-0.948	
(g)					1.800(1.014)	0.257	
(h)		ks	kp	$k'p$		-1.589	-0.991
		$2p$	kd	$k'd$		-0.543	-0.372
(i)		ks	kp			0.767	0.589
		kd	$2p_{0,-1}^+$			0.689	0.447
		$2p^\pm$	kd			3.776	2.637
(j)					0.402	0.441	
(k)					-1.403	-0.938	

tion. These field-gradient contributions come from changes in the $2p$ radial distribution which are induced by $2s-2p$ radial correlation. That is, the $2p$ orbital undergoes a modification in its radial structure due to correlation with the $2s$ orbitals and this results in contributions to R .

From the other diagrams in Fig. 6 we observe that only two involve $1s-2p$ correlation [(6a)], whereas all the rest result from $2s-2s$ or $2s-2p$ correlation. This, of course, reflects the importance of intrashell correlations in boron. Most of these diagrams also make leading contributions to the magnetic-orbital and spin-dipolar hyperfine interactions in boron.^{4,12} In general, the electronic structure of the open-shell system, boron, is very sensitive to L -shell correlations and to the availability of unoccupied $2p$ states for virtual excitation. Thus any accurate theoretical treatment of this system must account for these influences on the electronic wave function.

To summarize, the results of our LCMBPT calculation of the quadrupole shielding factor are given in Table II according to different levels of approximation and orders of perturbation. Column I has only bare-diagram contributions (except, of course, that the usual potential modification to the $1s$ energy has been taken.) Column II reflects all the modifications to the large $2s-2s$ diagram in Fig. 5 and the corresponding modifications of the two structurally related diagrams in Fig. 6 mentioned above. Column III contains contributions from the fully modified diagrams (that is, ladderization plus renormalization-like effects). Unless otherwise stated we shall henceforth refer to our final results as those of Column III. It is seen that, in second order, it is the (1, 1) type of diagrams which have the larger net contribution to R . Actually, of the net 6.17% contribution from second order, 3.87% is from the $2s-2s$ diagram of Fig. 5 with the remainder, 2.30%, coming from other (1, 1) diagrams. The fact that (1, 1) is substantially larger than (0, 2) again emphasizes that the electronic structure of

TABLE II. Summary of contributions to R (in percent). Column I has bare diagrams only. Column II has the fully modified diagram of Fig. 5 and the two structurally related diagrams of Fig. 6. Column III has fully modified versions of all diagrams in Fig. 6.

	I	II	III
(0, 1)	4.52	4.52	4.65
(1, 1)	16.27	7.21	6.17
(0, 2)	0.28	-0.56	-0.93
$\Sigma = (1, 1) + (0, 2)$	16.55	6.65	5.24
(0, 1) + Σ	21.07	11.17	9.89

boron is strongly influenced by correlation (especially in the L shell). Thus the quadrupole shielding constant receives about half of its magnitude from the single-particle angular polarization effect represented by the fully modified (0, 1) diagrams and the remainder is primarily due to the influence of correlation on the open-shell structure.

The net theoretical value of $R = 9.89 \times 10^{-2}$ is estimated to have a maximum uncertainty of about 10% of R . Thus, including this estimate of error, our theoretical quadrupole shielding constant for $B(2P_{3/2})$ can be quoted as $R = 0.0989 \pm 0.0099$ leading to a net $q = 0.27957 \pm 0.00276$ a.u. The range of error we have quoted covers the contributions of ladders and other modifications to the remaining smaller second-order diagrams plus possible significant higher-order diagrams not already included in the modifications to the diagrams of Figs. 5 and 6. The positive sign of R , of course, means that the ground-state electric field gradient q_J is smaller (i.e., shielded) than the bare Hartree-Fock contribution (see Table III).

We conclude this section with estimates of the nuclear quadrupole moments of the boron isotopes. The nuclear quadrupole coupling constant b_J has been accurately measured^{13,14} for B^{11} and the ratio of coupling constants for B^{10} to B^{11} has also been established.¹⁵ Thus from the relationship, $b_J = eQq_J$, we find the nuclear quadrupole moments Q as given in Table III in barns. The estimated error for the quadrupole moments is composed of both the theoretical uncertainty in q_J and the experimental error in b_J values. Our value of q_J and the nuclear quadrupole moments are found to be in excellent agreement with those obtained by Nesbet¹⁶ using a variational many-body procedure including some three-particle correlation. Nesbet has calculated $q = 0.28215 \pm 0.00074$ a.u.,

TABLE III. Final values for the field gradient for the $^2P_{J=3/2}$ state of boron. The resulting nuclear quadrupole moments for isotopes ^{10}B and ^{11}B are given (in b).

Quadrupole shielding constant		
$R_J: 0.0989 \pm 0.0099$		
Electric field gradient		
$q_J: 0.27957 \pm 0.00276$ a.u.		
$(9.0619 \pm 0.0896) \times 10^{14}$ esu/cm ³		
Boron isotopes	b_J/h (MHz)	Q (10^{-2} b)
^{11}B	2.6927 ± 0.0010^a	4.099 ± 0.047
^{10}B	$(2.084 \pm 0.002)b_J(^{11}B)^b$	8.543 ± 0.104

^a References 13 and 14.

^b Reference 15.

$Q(^{11}\text{B}) = (4.065 \pm 0.026) \times 10^{-2}$ b, and $Q(^{10}\text{B}) = (8.472 \pm 0.056) \times 10^{-2}$ b all being in very good agreement with our results. We shall compare the detailed contributions to R by these two methods in Sec. III.

III. DISCUSSION

In the last decade a number of *ab initio* calculations of the electric field gradient in boron have been performed with various improvements over the Hartree-Fock approximation. In Table IV we list the resulting value of the quadrupole shielding factor for the $^2P_{3/2}$ state of boron obtained by several different methods. The restricted Hartree-Fock (RHF), of course, has no shielding since it is the reference wave function defining R . The first improvement over the RHF was the removal of the double occupancy of spatial orbitals differing only in the spin projection quantum number. This leads to the spin-polarized Hartree-Fock (SPHF) which yields¹⁷⁻¹⁹ a small antishielding quadrupole-shielding constant. If in addition to dropping the equivalence restriction one also relaxes the angular momentum (i.e., central field) symmetry restriction on occupied atomic orbitals one has the unrestricted Hartree-Fock (UHF) scheme. Here the principal effect of angular polarization of s orbitals by d admixture is accounted for and the resulting R is substantially improved.¹⁹ On the other hand, the Sternheimer procedure⁹ also accounts for the relaxing of the symmetry restriction by direct perturbation to the Hartree-Fock equations. A third scheme yielding approximately the same shielding constant as the UHF and Stern-

heimer procedures is a configuration-interaction (CI) function constructed from the RHF configuration plus all singly excited symmetry-adapted configurations. This is called the polarization wave function²⁰ (PWF) and accounts for the spin and orbital polarization of the RHF orbitals while retaining the L - S eigenfunction property (as opposed to the UHF wave function). It is clear that these three methods account for the angular polarization contribution to R in agreement with the (0, 1) diagrams of the LCMBPT method (Fig. 2). The first-order (FO) wave function²¹ improves on the PWF method by including, in addition to the singly excited configuration, all L - S configurations which are doubly substituted but have at least one electron in an unoccupied $2p$ orbital. In particular, this method includes the so called "near-degeneracy" configuration, $1s^2 2p^3$, discussed in connection with the large diagram in Fig. 5. The FO wave function makes a substantial improvement by including this important correlation effect in the calculation of R . Thus, it is somewhat surprising that a CI wave function²² composed from 187 configurations (i.e., 1292 determinants) which also includes this near-degeneracy configuration as well as all types of double and even some triple and quadrupole excitations leads to a shielding constant of only 4.59×10^{-2} . This elaborate wave function, which gives 88% of the correlation energy for boron, demonstrates how sensitive the CI procedure is to the choice of basis functions and configurations even when a very large number of both are taken.

The variational Bethe-Goldstone (BG) formulation of the CI procedure^{12,16} attempts to overcome some of these difficulties by considering separately that class of symmetry-adapted configurations which arises from the virtual excitations of a specific subset of occupied orbitals. For example, only those symmetry-adapted configurations in which one or both members of a specific pair, (ij), of occupied orbitals (i or j) is replaced by a virtual orbital are to be considered in determining the contribution of this pair to a specific property. Furthermore, the set of virtual orbitals appropriate for such a subset can be extended until some degree of convergence in the property being computed is achieved. This procedure is based on the additivity of the various increments which has been brought into question by previous analyses.^{23,24} Nevertheless, the BG method has obtained very good results¹² for the magnetic hyperfine structure and the quadrupole shielding constant. The latter is 0.0904 which is in excellent agreement with our calculation. Since the contributions to R have been classified by configurational excitations, it is possible and very interesting to make a detailed

TABLE IV. The quadrupole shielding parameters R (in percent) obtained by several different theoretical methods.

Method	R
RHF	0.0
SPHF ^a	-0.80
UHF ^b	4.18
Sternheimer ^c	4.78
PWF (CI) ^d	4.13
First-order wave function (CI) ^e	11.90
Full CI (187 configurations) ^f	4.59
Variational BG (CI) ^g	9.04
LCMBPT ^h	9.89

^a References 17-19.

^b Reference 19.

^c Reference 9.

^d Reference 20.

^e Reference 21.

^f Reference 22.

^g References 12 and 16.

^h This work.

comparison with our results when the diagrams are appropriately regrouped.

The class of diagrams which contributes to, say, the $(1s)$ net increment for the electric field gradient is determined as follows. This set corresponds to all diagrams in which a single excitation of $1s$ is made to a virtual orbital (usually d_0 type) and all those diagrams through second order in which symmetry-adapted excitations of the type $1s2p_1^+ - kl2p_m^\pm$ are made. These excitations in which the occupied $2p_1^+$ orbital is replaced by one of the unoccupied $2p_m^\pm$ orbitals are important for the \vec{L}^2 , \vec{S}^2 character of the eigenfunction as well as usually being energetically more favorable. For a pair excitation increment such as $(2s2p)$ we consider all calculated diagrams in which both $2s$ and $2p_1^+$ hole lines occur, provided that a unoccupied $2p$ orbital does not occur simultaneously with the occupied $2p_1^+$. In the latter case, this would belong to the $(2s)$ class of increments. For example, in Fig. 6(h) with $k_1 = 2p$, we have a $(2s)$ contribution, whereas if k_1 is not a $2p$ then this is a $(2s2p)$ diagram. Finally, there is a class of diagrams in which three different hole lines occur but with at most two simultaneously (that is, overlapping in time where time intervals progress vertically in our diagrams). This class of contributions is denoted, for example, by $(2s^22p)_2$ where the subscript 2 denotes that no more than pair excitations are being included here. Figure 6(d) is an example of this class. True dynamic three-particle effects involving simultaneous excitation have not been considered explicitly in the LCMBPT procedure for this property, although such effects have been included partially through the ladderization of the $2s$ - $2s$ correlation diagram in Fig. 5. In the BG calculation, the quoted $(2s^22p)_2$ contribution includes¹² the influence of dynamic three-particle correlations within the L shell.

Contributions to R are given in Table V according to these classifications. Over-all agreement between the two methods is very good. This is especially true for those contributions in which one or both $1s$ single-particle states participate. However, the two $(1s2p)$ contributions differ by 0.0037 or about 12%. Those contributions which are most sensitive to the details of the computational procedure, namely, $(2s)$, $(2s^2)$, $(2s2p)$, and $(2s^22p)_2$, are found to differ more in these cases but, in general, the relative contributions are in good agreement. In fact it is found that the sums of the four increments involving $2s$ and $2p$ are quite comparable with the LCMBPT method giving 7.4×10^{-2} and by the BG-CI method, 6.2×10^{-2} . The single-particle increment $(2s)$ is different from the corresponding $(0, 1)$ angular polarization total, -0.044×10^{-2} , because of additional contributions

TABLE V. Comparison of contributions to R classified by the type of single-particle states participating in the virtual excitations. The variational Bethe-Goldstone results are from Ref. 12.

Class	This work	BG-CI
$(1s)$	4.669	4.695
$(2s)$	2.404	1.801
$(1s^2)$	0.232	0.275
$(2s^2)$	5.690	5.851
$(1s2s)$	0.289	0.273
$(1s2p)$	-3.177	-2.809
$(2s2p)$	-2.214	-4.000
$(2s^22p)_2$	1.542	2.543
$(1s^22p)_2$	0.265	0.412
$(1s2s2p)_2$	0.191	0.412
Totals	9.892	9.041

in which the hole $2p$ goes into an unoccupied $2p$. Obviously such "symmetry-adapted" excitations are highly significant for the L shell whereas they have little effect on K -shell contributions. In contrast to the very small $1s$ -pair contribution, $(1s^2)$, the $2s$ pair is the largest in the table. This $(2s^2)$ classification is, in fact, primarily due to the $1s^22p^3$ configuration-type diagrams of Fig. 5 and the two in Fig. 6 which were mentioned above. These three $2s$ -pair correlation diagrams total 5.192×10^{-2} out of 5.690×10^{-2} . It is of interest to note that classifications $(1s2p)$ and $(2s2p)$ which are the only net antishielding increments arise primarily from pair correlation combined with a $2p$ radial modification contribution to the field gradient. Finally, those field gradient contributions in which all three of the L -shell electrons participate, namely $(2s^22p)_2$, are found to produce a net shielding effect of amount 1.542×10^{-2} in R . There are only two diagrams of this class in second order, namely, Fig. 6(d) and the one in which $2p_{-1}$ is any other virtual p orbital. Such diagrams again exemplify the influence on the field gradient of mutual correlation among the $2s$ electrons in conjunction with modification to the $2p$ radial distribution. The difference between the results for $(2s^22p)_2$ listed for the LCMBPT and BG calculations can partially be explained by the fact that the quoted results in the latter case also included explicit three-particle interactions as well as the effects included in our $(2s^22p)_2$ results. In the last two rows of Table V we have listed $(1s^22p)_2$ and $(1s^22s2p)_2$ from our diagrams obtained in the same manner as $(2s^22p)_2$. For the BG calculations, we have only listed the sum of $(1s^22p)_2$ and $(1s^22s2p)_2$ contributions derived from the results in Table IV of Ref. 12 by taking the difference of the results quoted under $(total)_2$ and $(total)_3$. These results

which include K -shell intershell interactions did not incorporate explicit three-particle effects in both BG and LCMBPT calculations and are found to be very small.

Use of this classification scheme provides us with a simple means of determining the relative contributions attributable to one-, two-, or more-particle excitations. The principal contribution to the electric field gradient is the bare $2p$ which yields $1 \times q_0$ (in a convenient measure). The other one-particle contributions, (1s) and (2s), give $-0.0707q_0$ and hence the total one-particle amount is $0.929q_0$. From two-particle excitations we find $-0.028q_0$ which actually is slightly too small because this amount contains some multiple-particle effects. Finally, based on an examination of the contributions to the renormalization of the princi-

pal second-order diagram (Fig. 5) we deduce a dynamic three-particle contribution of $+0.001q_0$ to the field gradient. An examination of other diagrams involving dynamic three-particle correlations leads us to expect that such effects are not expected to be larger than $0.002q_0$. Thus we conclude that after considering the important correlation corrections to the single-particle contributions, the higher-particle effects are essentially negligible to an amount on the order of about 10% of the total two-particle contribution.

Finally, we want to point out that our findings here are consistent with a similar analysis¹⁰ of the field gradient in the excited 3P state of beryllium in regards to the convergence of perturbation theory and the relative contributions to the electric field gradient.

¹R. M. Sternheimer, Phys. Rev. 80, 102 (1950); 84, 244 (1951); 86, 316 (1952).

²J. E. Rodgers, Ph.D. dissertation (University of California, Riverside, 1972) (unpublished).

³For a partial review, see R. E. Brown, S. Larsson, and V. H. Smith, Jr., Phys. Rev. A 2, 593 (1970).

⁴See also Refs. 12 and 17-22.

⁵H. P. Kelly, in *Advances in Chemical Physics*, Vol. XIV, edited by R. Lefebvre and C. Moser (Interscience, New York, 1969), p. 129.

⁶N. C. Dutta, Ph.D. dissertation (University of California, Riverside, 1969) (unpublished).

⁷In regard to the normalization convention adopted here, see T. Lee, N. C. Dutta, and T. P. Das, Phys. Rev. A 1, 995 (1970).

⁸As an indication of the accuracy of the numerical Hartree-Fock used here we note that the value of $q_0 = 0.31025317$ a.u. agrees very well with that obtained by Mann of 0.3102532. [J. B. Mann, reports No. LA-3690 and LA-3691 (Los Alamos Scientific Laboratory of the University of California, 1967)].

⁹R. M. Sternheimer and R. F. Peierls, Phys. Rev. A 4, 1722 (1971).

¹⁰S. N. Ray, Taesul Lee, and T. P. Das, Phys. Rev. A 8,

1748 (1973).

¹¹H. P. Kelly, Phys. Rev. 144, 39 (1968); 173, 142 (1968); 180, 55 (1969); also see Ref. 5.

¹²R. K. Nesbet, Phys. Rev. A 2, 1208 (1970).

¹³J. S. M. Harvey, L. Evans, and H. Lew, Can. J. Phys. 50, 1719 (1972).

¹⁴G. Wessel, Phys. Rev. 92, 1581 (1953).

¹⁵H. D. Dehmelt, Z. Phys. 133, 528 (1952); 134, 642 (1953).

¹⁶R. K. Nesbet, Phys. Rev. Lett. 24, 1155 (1970).

¹⁷W. A. Goddard III, Phys. Rev. 182, 48 (1969).

¹⁸D. A. Goodings, Phys. Rev. 123, 1706 (1961).

¹⁹S. Larsson, Phys. Rev. A 2, 1248 (1970).

²⁰H. F. Schaefer III, R. A. Klemm, and F. E. Harris, Phys. Rev. 176, 49 (1968).

²¹H. F. Schaefer III, R. A. Klemm, and F. E. Harris, Phys. Rev. 181, 137 (1969).

²²H. F. Schaefer III and F. E. Harris, Phys. Rev. 167, 67 (1968).

²³H. F. Schaefer III and U. Kaldor, J. Chem. Phys. 49, 469 (1968).

²⁴U. Kaldor, H. F. Schaefer III, and F. E. Harris, Int. J. Quantum Chem., Vol. II S, 13 (1968).